Available online at www.sciencedirect.com
SCIENCE DIRECT®
Journal of Theoretical Biology 229 (2004) 69–83
Journal of Theoretical Biology
www.elsevier.com/locate/jtbi

Periodic stimulus and the single cardiac cell—getting more out of 1D maps

Eric N. Cytrynbaum

Department of Mathematics, University of California, Davis One Shields Avenue, Davis, CA 95616, USA

Received 30 June 2003; received in revised form 19 February 2004; accepted 3 March 2004

Abstract

The response of an isolated cardiac cell to a periodic stimulus has traditionally been studied in terms of the duration of the action potential (APD) immediately following each stimulus. The APD approach offers explanations of several experimental observations, including the stability of the so-called 1:1 response which is thought to be relevant to the problem of spiral wave breakup and the onset of fibrillation. A discussion of some theoretical problems with the APD approach is given in order to motivate the derivation of a new type of map. This new one-dimensional map, which gives successive values of the prestimulus transmembrane potential instead of successive values of APD, relies on the presence of a one-dimensional slow manifold in the underlying dynamics. This slow manifold map extends the understanding offered by the APD approach to include an explanation of Wenckebach rhythms. In addition, the bifurcation structure of the map provides a unified description of the parameter dependence that agrees fairly well with experimental observation.

Keywords: Alternans; Wenckebach rhythms; APD; Slow manifold; Restitution curve

1. Introduction

The normal activation of cardiac tissue begins at the sino-atrial (SA) node which fires periodically, exciting the atrial tissue around it. The excitation propagates through the atria and reaches the atrio-ventricular (AV) node where the signal is transmitted to the ventricles. Normally, each firing of the SA node induces the excitation of the ventricles through this pathway. However, if the AV node is paced too rapidly or the tissue is unhealthy (suffering from ischemia, for example) this well coupled stimulus–response pattern can degenerate into any one of a number of pathological coupling patterns (Yehia et al., 1999).

One avenue of research on these rhythms has focused on the interplay between the dynamic behavior of individual cells and the electrotonic coupling that occurs between cells through gap junctions (Cherry and Fenton, submitted for publication; Cytrynbaum and Keener, 2002; Echebarria and Karma, 2002). Although coupling certainly plays an important role, the study of isolated cells focuses on the simplest of excitable systems and, in this case, provides a great many explanations for the observed rhythms. Several experimental studies have shown that spatially uniform systems (either small pieces of tissue (Guevara et al., 1984; Hall et al., 1999) or isolated ventricular myocytes (Delmar et al., 1989b; Guevara et al., 1989; Yehia et al., 1997, 1999)) can exhibit response patterns analogous to those referred to above. In these studies, it is observed that if the frequency of pacing is sufficiently low, the response of the cell is identical with each stimulus. This type of rhythm is referred to as a 1:1 rhythm where the first 1 indicates one stimulus and the second 1 indicates one superthreshold response. If the frequency is increased beyond some critical value, the responses vary from one stimulus to the next generating a 2:2 rhythm, sometimes referred to as alternans. The appearance of these two distinct superthreshold responses is understood to correspond to a loss of stability of the 1:1 rhythm.

Although the motivation for these studies is most easily explained in terms of observations of AV node conduction anomalies, Hall et al. offer a different motivation for their experiments (Hall et al., 1999). Their goal is to understand the stability of the 1:1 rhythm with the hope that it will shed light on the

E-mail address: cytryn@math.ucdavis.edu (E.N. Cytrynbaum).

0022-5193/$ - see front matter © 2004 Elsevier Ltd. All rights reserved.
doi:10.1016/j.jtbi.2004.03.004

problem of spiral wave breakup. This idea led to the formulation of the restitution hypothesis (Karma, 2000). In cardiac tissue that is sustaining a reentrant arrhythmia, each cell fires periodically with a period determined by the circulation of the reentrant signal. The restitution hypothesis proposes that the question of stability for reentrant arrhythmias can be reduced to that of stability of the 1:1 response for a single cell (either in isolation or in tissue), although the details of this connection are not completely understood and are the subject of current debate (Ideker et al., 2002; Gilmour, 2002). Nonetheless, through the restitution hypothesis, the study of isolated ventricular myocytes under periodic stimulation becomes important in understanding reentrant arrhythmias as they provide a model system for the more complicated problem of cells in tissue. It should be noted that the value of single cell studies is limited as the role of spatial coupling in tissue is often significant (Cytrynbaum and Keener, 2002; Cherry and Fenton, submitted for publication; Echebarria and Karma, 2002). Despite this, it is worth building a more complete understanding of the simple problem of isolated cells in hope that it will shed light on the more complicated scenario of tissue dynamics.

The approach to understanding the stability of the 1:1 rhythm taken in many studies, both experimental and theoretical (Delmar et al., 1989a, b; Fox et al., 2002; Guevara et al., 1984; Hall et al., 1999; Lewis and Guevara, 1990; Nolasco and Dahlen, 1968; Otani and Gilmour, 1997; Tolkacheva et al., 2003; Yehia et al., 1997, 1999), is to focus on the duration of the excited phase referred to as the action potential duration (APD). A common assumption, referred to here as the APD assumption, is that the duration of an action potential in a periodically stimulated cell is a function of the period of time between the end of the previous action potential and the beginning of the current one. This recovery period is referred to as the diastolic interval (DI) (see Fig. 1).

Although there is evidence that the assumption is not truly valid (a fact often explained in terms of memory effects (Cherry and Fenton; Fox et al., 2002; Tolkacheva et al., 2003)), it is generally a good approximation and provides an elegant theory that explains many of the experimental observations.

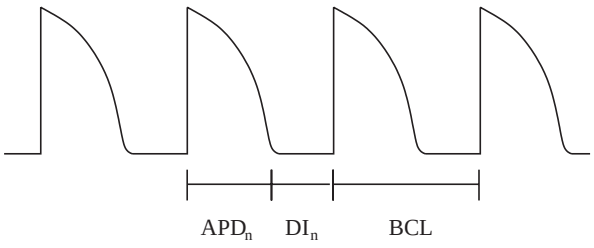

Fig. 1. A schematic representation of the transmembrane potential of a cell under periodic stimulus. An excited phase is called an action potential (AP) and its duration is the APD. The recovery period between APs is the diastolic interval (DI).

The assumption allows for the definition and study of a one-dimensional map given by $\mathrm{APD}_{n+1} = g(\mathrm{DI}_n)$. The function g, referred to as the restitution curve, is often defined by fitting an exponential function to experimental data. To generate a map from APD_n to APD_{n+1}, DI_n is computed as $\mathrm{BCL} - \mathrm{APD}_n$ where BCL is the stimulus period or basic cycle length. Stability of the 1:1 rhythm is equivalent to the condition $|g'| < 1$ where the slope is evaluated at the fixed point.

Thus, as shown by Guevara et al. (1984), the APD map offers an explanation for the loss of stability of the 1:1 and the appearance of a 2:2 rhythm through a period doubling (or flip) bifurcation. The added assumption that there is a minimum DI below which a cell does not respond to stimulus predicts the presence of a 2:1 rhythm which exists bistably with the 1:1 and 2:2 rhythms. These phenomena have also been observed in experiments (Guevara et al., 1984; Hall et al., 1999; Yehia et al., 1999).

Despite these successes, the APD map does have its limitations. For example, even when the map is defined by fitting the restitution curve to experimental data, quantitative details fail to agree. These include the location of the point at which stability is lost (Guevara et al., 1984; Hall et al., 1999; Fox et al., 2002) as well as details of the hysteretic loop (Hall et al., 1999; Yehia et al., 1999). Furthermore, the existence of the so-called Wenckebach rhythms, described in more detail later, cannot be explained in the context of an APD map, at least if the APD map is derived from or even consistent with an ODE type model.

These failures have stimulated attempts to define a two-dimensional map that extends the APD approach by introducing a memory variable (Chialvo and Jalife, 1990; Fox et al., 2002; Otani and Gilmour, 1997) or, in one case, a generalized one-dimensional map with explicit dependence on BCL (Tolkacheva et al., 2003). These memory models successfully extend the explanatory power of the APD map in a few directions. However, many questions remain unanswered including an explanation of the ionic mechanisms underlying memory and, closely related to this last point, the connection between (if not a derivation of) these memory models and ionic ODE models. Although the question of ionic mechanisms is not directly addressed in this paper, a framework for exploring that question, which can be generalized to ionic models, is constructed.

In this paper, starting from an ODE model for excitability, three related one-dimensional maps are defined. The first map is derived from a piecewise linear FitzHugh–Nagumo (FHN) system of ODEs in the singular limit ($\varepsilon \to 0$). This singular ODE system satisfies the APD assumption and leads to a map that is essentially the well-studied exponential APD map.

Improving on this map, a second map is derived from a generic FHN system but in this case, not using the singular system. Although this non-singular system fails to satisfy the APD assumption, we can derive a one-dimensional map that offers an explanation of the Wenckebach rhythms. In fact, by introducing a simplified version of this map (the third map), we can construct a fairly detailed bifurcation diagram including regions of existence and stability of these rhythms. Although these last two "improved" maps are derived from FHN dynamics and cannot be considered physiologically accurate, the idea underlying their derivation is applicable to more physiological ionic models. If a similar map can be derived from one of the more physiological ionic models (for example, see Beeler and Reuter, 1977 and Luo and Rudy, 1991, 1994), it is likely that more accurate quantitative predictions can be made. Although the successful derivation of an improved one-dimensional map from the FHN model does not necessarily rule out the need for a higher dimensional map, it certainly suggests that more analysis of ionic models is required before dismissing the one-dimensional approach. Interestingly, if a two- (or higher-) dimensional map is required to properly explain cardiac cell dynamics, the reduction technique introduced here is capable of providing such a map and, in doing so, offers an ionic basis for the notion of a memory variable.

2. An experimental bifurcation diagram

In a recent publication, Yehia et al. give a comprehensive discussion of the types of rhythms that an isolated cardiac cell can demonstrate under regular pacing (Yehia et al., 1999). A cell isolated from rabbit ventricular muscle was stimulated periodically and the resulting sequence of APDs was measured. The two parameters of interest were the BCL and the amplitude of the periodic stimulus.

It was found that for sufficiently large BCL, the response pattern settled down to a 1:1 rhythm. For sufficiently small BCL, the measured APD alternated between that of a full action potential and that of a subthreshold response with essentially no action potential, in other words, a 2:1 rhythm (see Fig. 2).

These two rhythms occur over a large range of stimulus amplitudes and are relatively easy to understand. For large BCL, the cell has sufficient time to recover from the previous action potential before the next stimulus. This allows the cell to undergo an identical action potential with each stimulus. The 2:1 rhythm develops because of a lack of recovery time between stimuli. Following a full action potential, the cell requires more time than allowed by the stimulus period in order to recover excitability. A stimulus delivered during this unrecovered stage elicits a subthreshold response.[1]

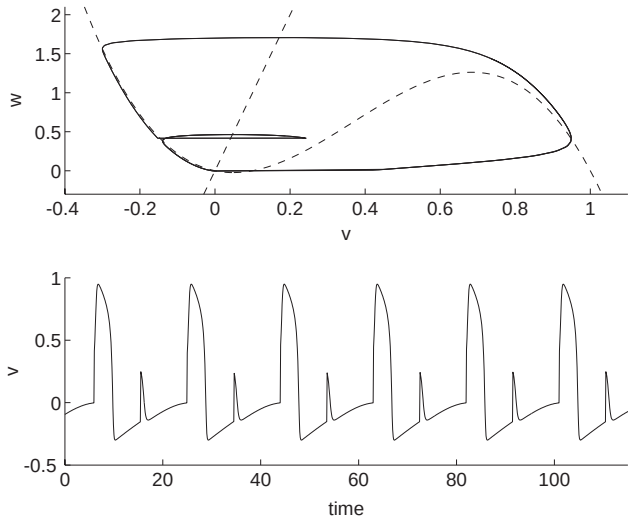

Fig. 2. A 2:1 rhythm found in the FHN system with a periodic stimulus (BCL = 9.5), analogous to the experimentally observed 2:1 rhythm. Top: FHN phase plane showing the trajectory of a 2:1 rhythm, a full action potential and a subthreshold response. Bottom: The same rhythm plotted as a function of time.

More subtle and interesting dynamics appear in between these two extremes. The rhythms that appear at intermediate pacing frequencies can be divided into three general classes based on stimulus amplitude.

For large stimulus amplitude and decreasing BCL, the 1:1 rhythm gives way to a sequence of APDs that alternate in amplitude. Unlike the 2:1 rhythm, which appears for smaller BCL, this 2:2 rhythm (alternans) is characterized by two distinct superthreshold responses of different duration.

For intermediate stimulus amplitude, a direct transition from 1:1 to 2:1 is observed with no other rhythm appearing in between. Furthermore, Yehia et al. show that there exists an interval of BCL in which the 1:1 and 2:1 rhythms coexist and form a hysteretic loop (Yehia et al., 1999). This kind of bistability has been found between the 2:2 and 2:1 rhythms as well (Hall et al., 1999). See Figs. 3.

For low stimulus amplitude, the 1:1 rhythm is replaced by $N+1:N$ rhythms ($N \geqslant 2$) as BCL decreases. This means there are $N+1$ stimuli but only N superthreshold responses. This type of rhythm is referred to as a Wenckebach rhythm.

[1] If the period of pacing is shortened even further, stimuli begin to overlap with the plateaus of action potentials and more complicated rhythms result. For the present study, we avoid stimulus protocols with such short periods.

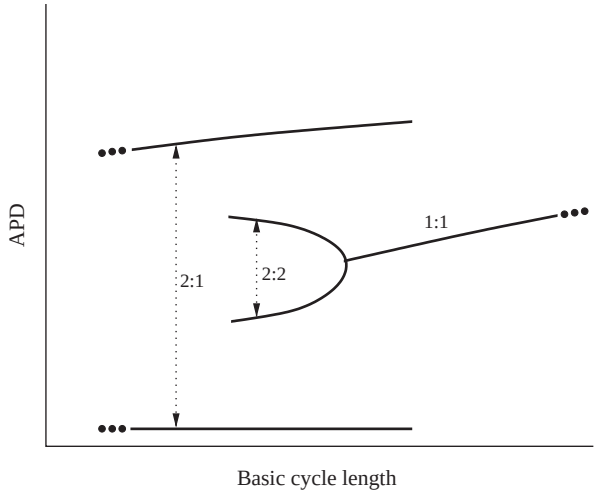

Fig. 3. A schematic representation of the bistability observed experimentally. Note the bistability of the 1:1 and 2:1 rhythms and of the 2:2 and 2:1 rhythms. See Guevara et al. (1984), Yehia et al. (1999) and Hall et al. (1999) for actual experimental bifurcation diagrams.

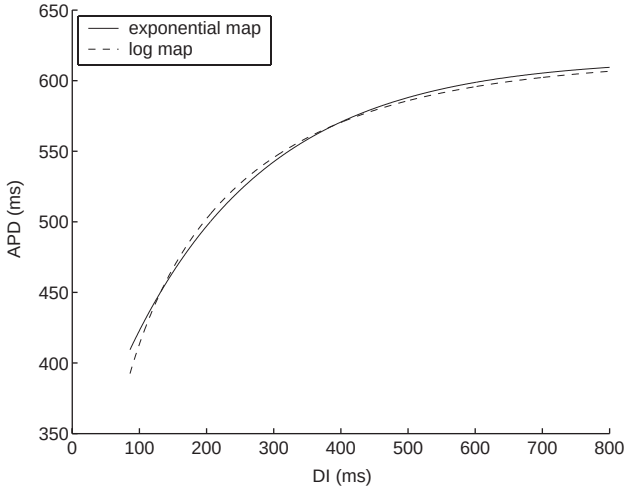

Fig. 5. The solid curve is the exponential map with parameters typical of experimental fits ($\mathrm{APD}_{\max} = 616$ ms, $A = 313$ ms, $\mathrm{DI}_{\min} = 86$ ms and $\tau = 207$ ms) (Hall et al., 1999). The dashed curve is the log map with parameters chosen, as described in the text, that provide the best fit ($\eta = 0.69$, $s = 0.74$, $\mu = 269$ ms and $a = 0.036$).

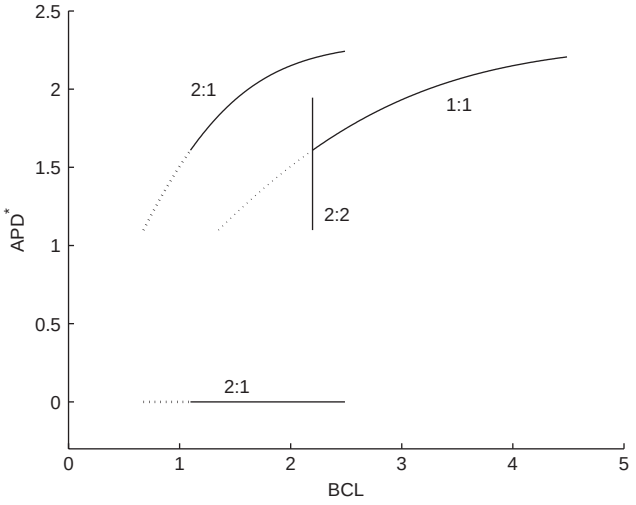

Fig. 4. Bifurcation diagram for the log map with $\eta = 1$, $s = 0.8$ and $a = 0.1$. The solid curves are stable and dashed curves are unstable.

3. The one-dimensional APD iteration model

One of the fundamental assumptions of the APD map approach, the APD assumption, is that APD is a function of the preceding recovery period or DI only. If the cell is assumed to be either excited or recovering, then $\mathrm{BCL} = \mathrm{APD} + \mathrm{DI}$ and $\mathrm{APD}_{n+1} = g(\mathrm{DI}) = g(\mathrm{BCL} - \mathrm{APD}_n)$. In the case of subthreshold responses, where $\mathrm{BCL} - \mathrm{APD}_n$ is less than some minimum DI required to reestablish excitability, it is assumed that the subthreshold stimulus has no effect on the cell and the cell receives an extra BCL in which to recover. Thus, if the cell undergoes N unsuccessful stimuli before firing, $\mathrm{DI} = N \cdot \mathrm{BCL} - \mathrm{APD}$ and $\mathrm{APD}_{n+1} = g(N \cdot \mathrm{BCL} - \mathrm{APD}_n)$.

The typical choice for g is an exponential of the form

$$g(\mathrm{DI}) = \mathrm{APD}_{\max} - A\mathrm{e}^{-\mathrm{DI}/\tau}, \quad \mathrm{DI} > \mathrm{DI}_{\min}, \tag{1}$$

where $\mathrm{APD}_{\max}$, A, τ and $\mathrm{DI}_{\min}$ are parameters to be fit. We refer to this map as the exponential map.

With a careful choice of parameters, this map can demonstrate the progression of 1:1, 2:2 and 2:1 rhythms with the hysteretic properties observed in experiments. Other parameter choices can show a direct transition from 1:1 to 2:1. Unfortunately, it is not clear how the parameters of the model relate to experimental parameters (for example, stimulus amplitude).

As mentioned earlier, the map is incapable of giving quantitative fits to actual cell data (Hall et al., 1999; Yehia et al., 1999); nor does it explain the existence of Wenckebach rhythms. Moreover, Hall et al. fit the parameters in (1) to their data and find that fixed points that were stable in their experiments correspond to fixed points of the map for which $g'(\mathrm{DI}) > 1$. According to the theory of one-dimensional maps, these two facts are inconsistent.

A common conclusion drawn from the shortcomings mentioned is that a complete understanding of the dynamics requires at least a two-dimensional map where the first variable is APD and the second is a memory variable that keeps track of the history of the system (Chialvo and Jalife, 1990; Fox et al., 2002; Otani and Gilmour, 1997). However, one possible explanation for the observed inconsistencies, at least in experiments on intact tissue in contrast to isolated cells, derives from the influence of cell–cell coupling on the stability of

reentrant rhythms. Electrotonic effects have been shown to modify the stability condition by introducing dependence on conduction velocity allowing for stable rhythms despite slopes greater than unity (Cytrynbaum and Keener, 2002; Cherry and Fenton, submitted for publication). Another possibility, described in a recent publication by Tolkacheva et al. (2003), is that by neglecting explicit dependence of APD on BCL, the slope of the APD–DI curve (in contrast with the slope of the actual map) gives an inaccurate stability condition.

To better understanding the shortcomings of the exponential map, starting from the singular FHN system, the following one-dimensional map is derived in the appendix:

$$\mathrm{APD}_{n+1} = h(\mathrm{DI}_n) = \mu\eta \ln\left(\frac{1-(1-a)\mathrm{e}^{-\mathrm{DI}_n/\mu}}{a}\right),$$

where a is the excitation threshold, μ is the time constant for recovery, η is the ratio of the time constant associated with the excited phase to μ and $\mathrm{DI}_n = \mathrm{BCL} - \mathrm{APD}_n$. As shown in the appendix, this map is qualitatively and, to a large extent, quantitatively equivalent to the exponential map. As the FHN model is useful in the context of cardiac tissue in a qualitative sense only, it is not surprising that a map derived from it gives a poor fit to cardiac cell data. In Section 4.1, we derive a one-dimensional map from the FHN model that explains the presence of Wenckebach rhythms. Finally, in addition to the ideas suggested in the previous paragraph, the inconsistency of fixed point stability and $g'(\mathrm{DI}) > 1$ can be explained by the fact that g is not well defined for cardiac tissue rather than by the lack of a second dynamic variable. In fact, the map derived in Section 4.1 is also a one-dimensional map but, unlike $g(\mathrm{BCL} - \mathrm{APD})$, it does not have the feature that a change in BCL amounts to a horizontal shift of the map (as addressed in Tolkacheva et al. (2003) by the introduction of explicit BCL dependence in the map). For cardiac tissue, any successful map must be calculated separately for each BCL since it depends on BCL through more than just its dependence on DI (Elharrar and Surawicz, 1983). If cardiac tissue demonstrates the slow manifold structure that characterizes the FHN system (explained more carefully in Section 4.1), then the "memory" of the system can be summarized by BCL, a parameter of the protocol, without appealing to a second map variable.

To emphasize the key point of this section, the problems with the APD map are not necessarily related to the details of the fits used to define it nor the absence of a memory variable. Reducing the high-dimensional and complex dynamics of cardiac cells to a single variable, in particular one that is not a state variable of the system, exposes one to the possibility of missing crucial features. The log map and the ODE system from which it is derived offer a unique case in which APD is equivalent to a state variable. Moreover, the structure of the system is sufficiently simple that this single state variable carries all the dynamical information of the system. In general, a single state variable is only sufficient if the structure of the system is sufficiently simple, as discussed in next section.

4. Building a better map

A careful look at some of the experimental data, particularly relating to Wenckebach rhythms, reveals some features that are missing in the log and exponential maps. A Wenckebach rhythm consists of N super-threshold responses followed by a final subthreshold response. The first N responses are characterized by a beat to beat decrease in amplitude and increase in activation delay (Delmar et al., 1989b). As Wenckebach rhythms are periodic, this monotone behavior must switch after the final skipped beat, returning to the first full response. Thus, a map capable of explaining Wenckebach rhythms is necessarily non-monotonic.

This feature of Wenckebach rhythms can be found in the FHN model with cubic right hand side (as depicted in Figs. 6 and 7):

$$v_t = \frac{1}{a}v(1-v)(v-a) - w, \tag{2}$$

$$w_t = \varepsilon(v - \gamma w) \tag{3}$$

with $a = 0.1, \varepsilon = 0.7, \gamma = 0.1$ and a shock amplitude of $s = 0.4$. Because of the decreasing monotonicity of both the log and exponential maps, they are incapable of

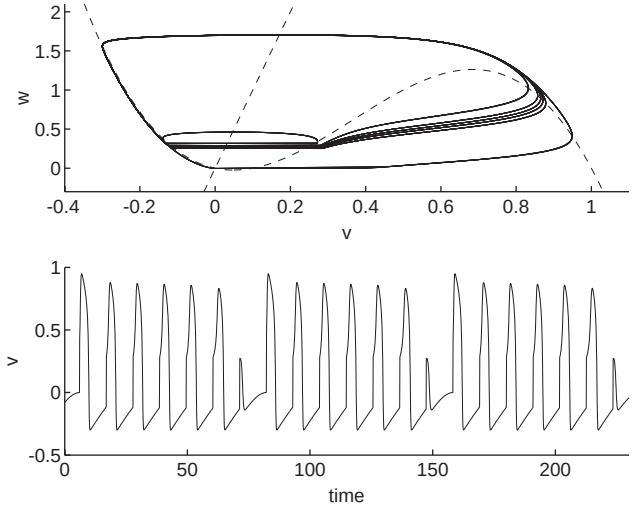

Fig. 6. The phase plane (top) and temporal evolution (bottom) of the FHN system under periodic stimulus showing a 7:6 rhythm. Note the successive approach to the middle nullcline from below until a final sub-threshold response. Although there is no true threshold in the FHN model, a weak concept of threshold divides the sixth and seventh stimuli (BCL = 10.87).

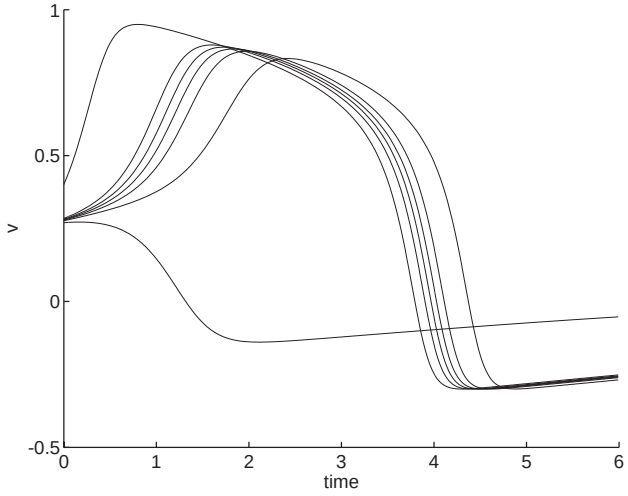

Fig. 7. Successive Wenckebach action potentials from Fig. 6 aligned by the moment of stimulus and superimposed to demonstrate the increasing activation delay as seen experimentally (Delmar et al., 1989b). Note the successive decrease in amplitude and increase in APD until the final sub-threshold response.

generating Wenckebach rhythms of this type. Somewhere between the cubic model used to generate the tracing in Fig. 6 and the map derived in the appendix, Wenckebach rhythms were lost. Experimental studies have uncovered such nonmonotonicities in the restitution curve of cardiac cells (Chialvo and Jalife, 1990; Watanabe et al., 1995) and some theoretical work has focused on the question of restitution curves with regions of negative slope (Panfilov and Zemlin, 2002; Qu et al., 1997; Fenton et al., 2002) but these studies did not draw any connection to Wenckebach rhythms. Early work on Wenckebach rhythms by Guevara et al. suggests a form for a finite difference map based on experiments with rabbit ventricular myocytes that invokes negative restitution (Guevara et al., 1989).

The phase plane in Fig. 6 exhibits the feature that successive responses start successively closer to the middle branch of the cubic shaped nullcline, the structure that is responsible for threshold-like behavior. Because of the proximity to this slow dynamic region, the upstroke is delayed more with each beat. This delay is similar to the experimental observation of increase in activation delay mentioned above (Delmar et al., 1989b) and is the key to getting the required non-monotonicity of the map.

A Wenckebach rhythm starts with a full action potential, uninfluenced by the middle nullcline. The next stimulus is applied when the cell has recovered just enough so that the stimulus puts it near the nullcline. It can either fall above the nullcline (subthreshold), in which case the rhythm is 2:1, or it can end up in the delay region. Despite a lower amplitude excitation, the delay in activation means that with the next stimulus, it is possible that the cell finds itself once more in the delay region. This process can be repeated generating higher order Wenckebach rhythms (as seen in Fig. 6). Numerical simulations of the FHN model, with parameters as given above, demonstrate the existence of Wenckebach rhythms of order as high as 19:18 (BCL = 10.92).

It should be noted that because of the delays near the middle branch of the cubic nullcline, APD is not a suitable variable for defining a map. In the singular limit, the state of the system is either excited or at rest leading to unambiguous definitions of both DI and APD. For $\varepsilon > 0$, the definitions are no longer clear cut. The usual method of defining APD experimentally is to choose a threshold value of v. The action potential begins when that value is first surpassed and terminates when v drops below it. The problem with implementing this definition when defining an APD map is that there are sometimes two distinct action potentials that have the same duration. This is necessarily true when the parameters are chosen in the range for which Wenckebach rhythms are seen but might also be true in other parameter regimes. This is demonstrated in Fig. 8 for which a family of initial conditions were chosen with the same initial v value but a variety of w values. The value of $v = 0.28$ was chosen such that the majority of pairs (v, w) were superthreshold thereby generating a diverse family of action potentials. At 10.87 non-dimensional time units later (this is the value of BCL that led to the 7:6 rhythm seen in Fig. 6), a stimulus was applied, generating a second family of action potentials (see Fig. 8a). For each initial condition, the second APD was plotted against the first APD giving the APD "map" (see Fig. 8b). Note that there is a nontrivial interval of APD_1 having two associated values of APD_2. The overall shape of the "map" is reminiscent of the usual

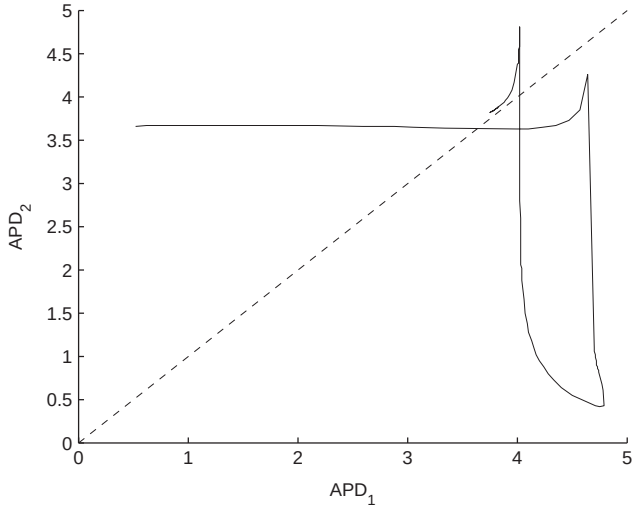

Fig. 8. The non-functional APD "map" calculated numerically by applying two successive stimuli to the FHN model with $s = 0.4$ and BCL = 10.87 using a family of initial conditions with $v = -0.12$ and $w \in [0, 0.4]$.

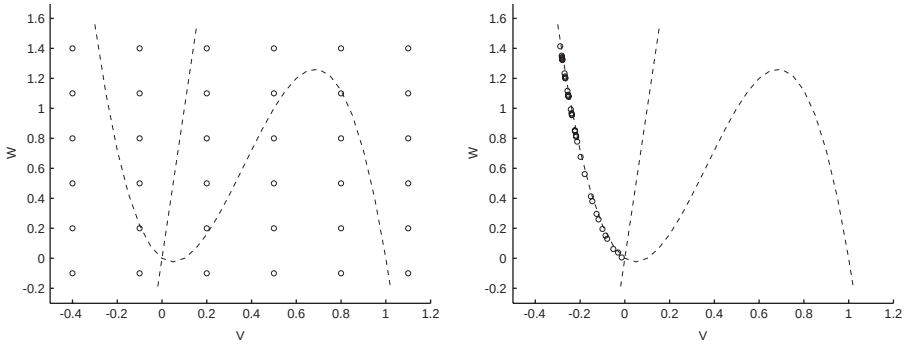

Fig. 9. Temporal evolution of a family of initial conditions, denoted by circles. The left panel shows the initial conditions. These were chosen to cover the region throughout which the state of a paced cell is likely to be found. The right panel shows a snapshot of the flow at $\tau = 5$ which is less than the lowest value of BCL used in this study. Note all initial conditions have converged to the slow manifold which lies almost, but not exactly, on the lower branch of the v nullcline.

restitution curve except for this multivalued interval. In fact, for larger initial values of v, relevant in the alternans parameter regime, the curve is generally functional (not shown) but in the range of v relevant to Wenckebach rhythms, it is necessarily non-functional. Although little direct evidence is currently available for a non-functional interval of this type in ionic models (Courtemanche et al., 1993) or in cardiac tissue, such a region is likely to be found when the state variables flow through regions of the state space that are crucial for the existence Wenckebach rhythms, in particular, regions near the higher dimensional analogue of the middle branch of the v nullcline.

Recall that in deriving the log map, the singular limit reduces the dynamics to two one-dimensional branches so there is no possibility of getting the non-monotonicity required for the existence of Wenckebach rhythms. In particular, the delay associated with the middle nullcline is absent.[2]

This one-dimensional shortcoming sounds as if it lends credence to the claim that a one-dimensional map is insufficient. The problem with the log map, and by association the exponential map, is that it is derived from ODE dynamics that are restricted to a one-dimensional manifold. However, the dimension of a map derived from an ODE system need not be the same as the dimension of the ODE system. For example, a Poincaré map derived from a two-dimensional flow is a one-dimensional map. Thus, it might be possible to improve on the log map without abandoning the simplicity of a one-dimensional map. To do so, we require a higher-dimensional ODE system that allows for the non-monotonicity of recovery described above while still maintaining reducibility to a one-dimensional map.

[2] Piecewise linear dynamics (with only two branches) are worse than cubic dynamics in that the delay region is missing, even for $\varepsilon > 0$, but in either case the singular limit calculation ignores the subtleties of that region.

Unlike a Poincaré map, which has a dimension one less than the ODE system from which it derives, any high dimensional system that has a one-dimensional slow manifold should be reducible to a one-dimensional map. Careful examination of an ionic model might uncover the appropriate one-dimensional slow manifold structure and allow for the derivation of a quantitative one-dimensional map using the technique described here. If, however, the slow manifold is two-dimensional (or higher), the system cannot be reduced to a one-dimensional map, in which case the technique presented here can be modified to derive the appropriate two-dimensional (or higher) map thus providing a rigorous derivation of a memory map when such a map is required. In the next section, we demonstrate this technique on the simpler and more tractable FHN model in the non-singular-limit case.

4.1. The slow manifold map

We have already seen that in the limit $\varepsilon \to 0$, the map derived from the FHN model lacks certain key features. However, if we take ε to be small but nonzero, the rapid, but not instantaneous, collapse to a slow manifold (see Fig. 9) provides the structure we require to derive an improved one-dimensional map. A similar approach to reducing a piecewise linear FHN model was used by Coombs and Osbaldestin (2000) to understand rhythms in the context of paced nerve cells.

Defining the map requires an analytical expression for the slow manifold. An equation that describes the shape (but not the temporal parameterization) of trajectories is given by

$$\frac{dw}{dv} = \varepsilon \frac{v - \gamma w}{f(v) - w}. \tag{4}$$

A (v, w) relation for any trajectory can be expressed as an asymptotic series in ε: $w = \mathscr{F}(v) = \mathscr{F}_0(v) + \varepsilon \mathscr{F}_1(v) + \varepsilon^2 \mathscr{F}_2(v) + O(\varepsilon^3)$. Using (4), the slow manifold can be approximated using a standard perturbation

calculation. The leading order terms of (4) give the following equation:

$$(f(v) - \mathscr{F}_0(v))\mathscr{F}_0'(v) = 0. \quad (5)$$

There are two options. If we assume $\mathscr{F}_0(v) \neq f(v)$ then $\mathscr{F}_0(v)$ is constant which corresponds to a trajectory on the fast manifold. We are interested in the slow manifold so we proceed with $\mathscr{F}_0(v) = f(v)$. The higher-order terms are calculated similarly:

$$\mathscr{F}_0(v) = f(v),$$

$$\mathscr{F}_1(v) = -\frac{v - \gamma f(v)}{f'(v)},$$

$$\mathscr{F}_2(v) = \frac{\mathscr{F}_1(v)(\gamma - \mathscr{F}_1'(v))}{f'(v)}.$$

Suppose the state variables of a theoretical FHN cell lie on or near the slow manifold. If a stimulus is applied to the cell, the point in the phase plane which represents its state is translated horizontally. From this new location, it is allowed to flow for BCL time units before the application of the next stimulus. This defines a map from the state of the cell prior to the first stimulus to the state of the cell prior to the second stimulus.

For sufficiently large values of BCL, the state of the cell sits on or near the slow manifold prior to each stimulus which allows for the definition of a one-dimensional map. Using the functional relationship $w = \mathscr{F}(v)$, we need only specify the v component of the prestimulus state vector. We can generate a sequence of prestimulus transmembrane potentials, v_n, satisfying $v_{n+1} = \mathscr{M}(v_n)$ where $\mathscr{M}$ is the map described in the previous paragraph, which we refer to as the slow manifold map.

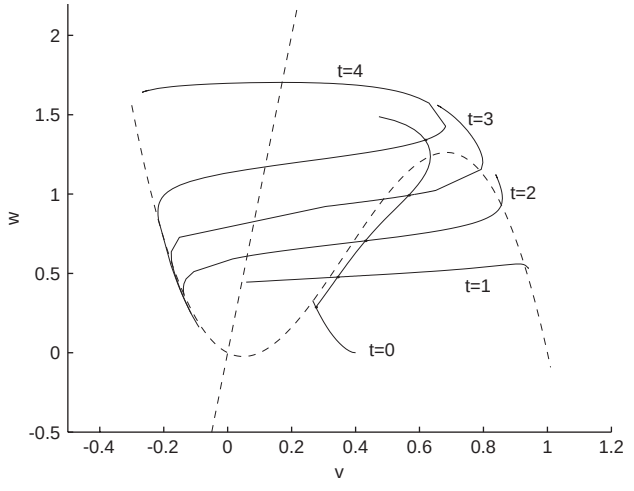

Fig. 10. This figure demonstrates the source of the non-monotonicity of the slow manifold map in the Wenckebach parameter range. A small section of the slow manifold and its poststimulus evolution (at five successive time points) is represented by the labeled solid curves. The transverse solid curve shows one of the "long delay" trajectories. On either side of this highlighted trajectory, other parts of the flow move faster, thereby creating the non-monotonicity when all points finally return to the slow manifold. Note that to allow for these long delays near the middle branch of the nullcline and, hence, Wenckebach rhythms, the stimulus amplitude must be small.

It is important to note, in light of earlier comments, that the slow manifold map relies on the two-dimensional nature of the FHN system. The flow is only restricted to a one-dimensional manifold in the latter part of its evolution. The freedom of the initial two-dimensional flow allows for differential time lags in the approach to the manifold to generate the nonmonotonicities that are crucial to finding Wenckebach rhythms (see Fig. 10).

5. Numerical representation of the map

This section gives a detailed description of the parameter dependence of the map $\mathscr{M}$, described in Section 4.1. The goal is to understand the experimental observations discussed in Section 2 to the extent that this is possible with a FHN based map. Earlier modeling approaches have been successful at explaining some of these observations including alternans (2:2 rhythms) and the hysteresis and bistability of the 1:1 and 2:2 rhythms with the 2:1 rhythm (Guevara et al., 1984; Nolasco and Dahlen, 1968). Wenckebach rhythms have not been as well explained by earlier models. Guevara et al. (1989) offer some preliminary ideas on the form a Wenckebach map must take, however, they do not succeed in relating this form to the general context of understanding the transition from a 1:1 rhythm to a 2:1 rhythm.

The accompanying diagrams were generated by explicitly calculating the map and its second iterate for particular parameter values on a course grid and then using a bisection method to accurately find the locations of all fixed points and period two solutions. The Wenckebach rhythms in Fig. 13 were calculated by iterating the map until steady solutions were achieved. Stability was determined by numerically calculating the slope at the fixed point or, for period two solutions, the product of the slopes. The extent to which this is an accurate means of determining stability in the original paced FHN model is related to the accuracy of the assumption that the slow manifold is one-dimensional but for the reduced map, it is a theoretically exact means of doing so. From the bifurcation structure, a unified explanation of the transitions between rhythms covering the full spectrum of alternans, hysteresis and Wenckebach rhythms can be given.

At relatively high stimulus amplitude ($s = 0.8$), the bifurcation diagram is essentially a simple supercritical flip bifurcation (not shown). The 1:1 rhythm is stable for high BCL and loses stability at BCL = 4.2. A 2:2 rhythm appears at the bifurcation point and gradually expands until it reaches what must be considered a 2:1 rhythm. There is no sharp transition between them nor

any bistability. Except for the lack of bistability, this appearance of a 2:2 rhythm at high stimulus amplitude is consistent with experiments.

Again consist with the observations of Yehia et al. (1999), at slightly lower stimulus amplitude ($s = 0.65$), the loss of stability of the 1:1 rhythm is a subcritical flip bifurcation generating an interval of bistability between the 1:1 and the 2:1 rhythm (Fig. 11). The steep transition in the map at around $v_n = -0.2$ reflects the large change in the length of time spent excited for stimuli on either side of the middle branch of the nullcline. This steep transition is successively more pronounced at lower stimulus amplitudes (see Figs. 12 and 13) due to longer delays for barely superthreshold stimuli.

For $s = 0.6$, the bifurcation diagram is almost the same as for $s = 0.65$ with the primary difference being that the 1:1 rhythm loses stability through a supercritical flip bifurcation allowing for a short interval on which a

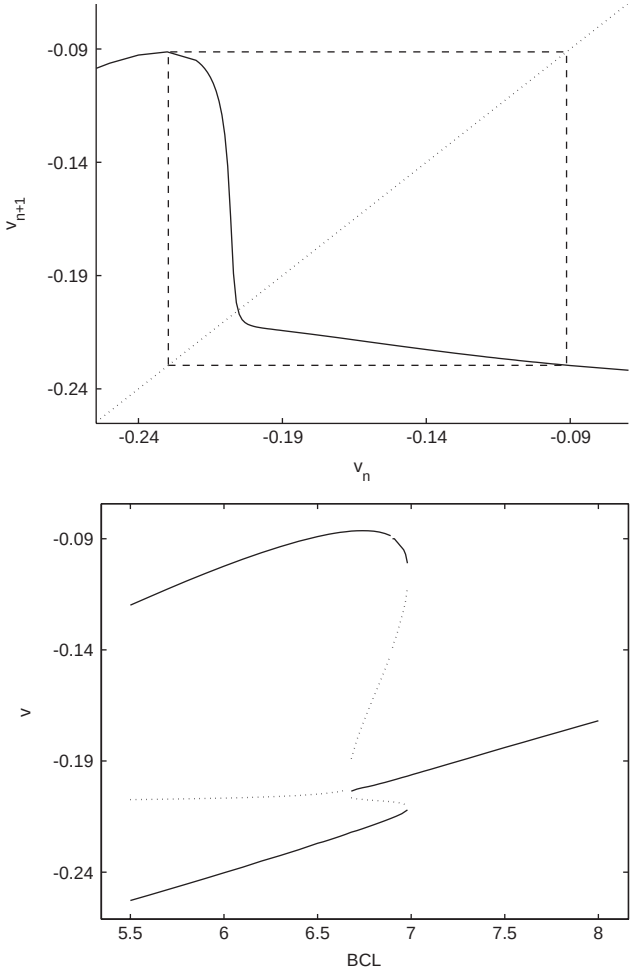

Fig. 11. The slow manifold map (top) for BCL = 6.4 and $s = 0.65$ and the corresponding bifurcation diagram (bottom) for $s = 0.65$. Top: the dashed curve represents the 2:1 rhythm and the fixed point is unstable. Bottom: the bifurcation diagram shows a subcritical flip bifurcation allowing for bistability between the 1:1 and 2:1 rhythms. The solid curves are the stable 1:1 and 2:1 rhythms. The dotted curves are the unstable 1:1 rhythm and an unstable period two rhythm.

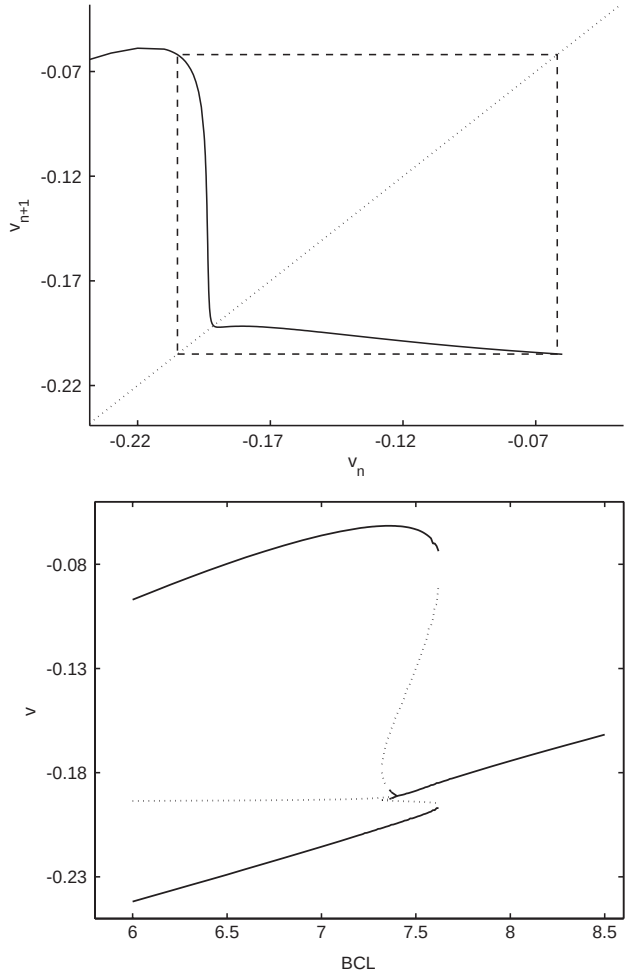

Fig. 12. The slow manifold map (top) for BCL = 7.4 and $s = 0.6$ and the corresponding bifurcation diagram (bottom) for $s = 0.6$. Top: the dashed curve represents the 2:1 rhythm and the fixed point is unstable but there is also a stable 2:2 rhythm (not shown on map). The difference between this case and $s = 0.65$ is the transition at around $v = -0.2$ is slightly steeper and the corner at the base of the transition is more pronounced. Bottom: the bifurcation diagram shows a supercritical flip bifurcation of the 1:1 rhythm leading to alternans. Both the 1:1 and 2:2 rhythms show bistability with the 2:1 rhythm.

stable 2:2 rhythm co-exists with a stable 2:1 rhythm as observed in experiments. Note that this difference arises from a slightly steeper transition near $v = -0.2$ and a sharper corner at the bottom of the transition (see Fig. 12).

For $s = 0.4$, the lowest value considered, we see a dramatic change in the map (see Fig. 13). The steep transition in the map is nearly a jump discontinuity and the sharp corner at its base, now a sharp spike, introduces the non-monotonicity required for Wenckebach rhythms. Changes in BCL essentially shift the map vertically so that at high values, the fixed point is on the flat section to the right and, as BCL decreases, the fixed point moves left causing two new (unstable) fixed points to appear as the spike crosses the identity line. One of these fixed points collides with the stable

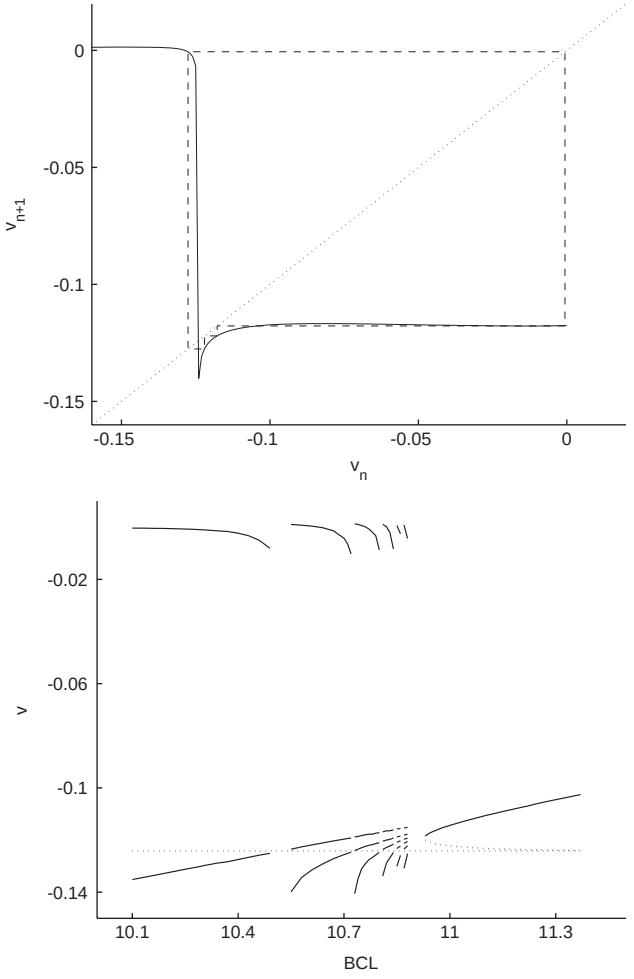

Fig. 13. The slow manifold map (top) for BCL = 10.77 and $s = 0.4$ and the corresponding bifurcation diagram (bottom) for $s = 0.4$. Top: the dashed curve represents the 4:3 rhythm and the fixed point is unstable. The transition is nearly a jump discontinuity and the corner has sharpened to a spike. Bottom: the bifurcation diagram shows multiple 1:1 rhythms due to the spike, only one of which is stable, and a sequence of Wenckebach rhythms has appeared.

fixed point leaving a narrow gap through which iterates "bounce" thus generating Wenckebach rhythms of relatively high order. A 4:3 rhythm is shown in Fig. 13. The bifurcation diagram shows a sequence of Wenckebach rhythms from 2:1 to 7:6. These rhythms were calculated by iterating the map until a steady rhythm was achieved so that only the stable rhythms are seen. Note that the structure of the map is as predicted by Guevara et al. (1989) although the one presented here is not an APD map.

It is interesting to note that there is no bistability between Wenckebach rhythms and, in fact, a short interval of BCL separates each rhythm from the next. The stable rhythms in between are complicated and interspersed with chaotic cycles. Although we do not rigorously address this claim of chaos, there is a structure similar to the well known Smale Horseshoe Map in the full FHN flow as can be seen in Fig. 10. In addition, the bifurcation diagram for $s = 0.5$ does not indicate the presence of Wenckebach rhythms but does show evidence of a period doubling cascade. At $s = 0.4$, this period doubling cascade is likely to occur in the spike although over an extremely short, and hence difficult to observe, interval of BCL due to the steep slopes in the spike. The appearance of rhythms through the spike is well described by the theory of unimodal maps (Stefan, 1977) and we merely leave it as a suggestion that many of the rhythms that appear in this range might be disappearing through the observed Wenckebach rhythms (see Section 6). In particular, the disappearance of the 3:2 rhythm at BCL = 10.5 (Fig. 13) indicates that a period three rhythm exists throughout a large interval of BCL which has implications for the existence of chaotic orbits (Li and Yorke, 1975).

6. Completing the bifurcation diagram

Now that the Wenckebach generating structure is clear, it is possible to clarify the details of the bifurcation diagram that were omitted in Fig. 13 by introducing a simplified version of $\mathscr{M}$. The following piecewise linear map captures the essential components of the slow manifold map in the Wenckebach regime (see Fig. 14).

$$M(x) = \begin{cases} M_1(x) = -\alpha x + \kappa, & x \leqslant 0, \\ M_2(x) = x + \kappa, & 0 < x \leqslant 1, \\ M_3(x) = 1 + \kappa, & x > 1, \end{cases} \tag{6}$$

where α and κ are parameters similar in their influence to s and BCL, respectively, in that increasing α steepens the transition (as does decreasing s) and decreasing κ (for $\kappa < 0$) increases the distance between the map and the identity line (as does decreasing BCL).

This map allows for explicit calculation of entire classes of solutions, in particular Wenckebach rhythms.

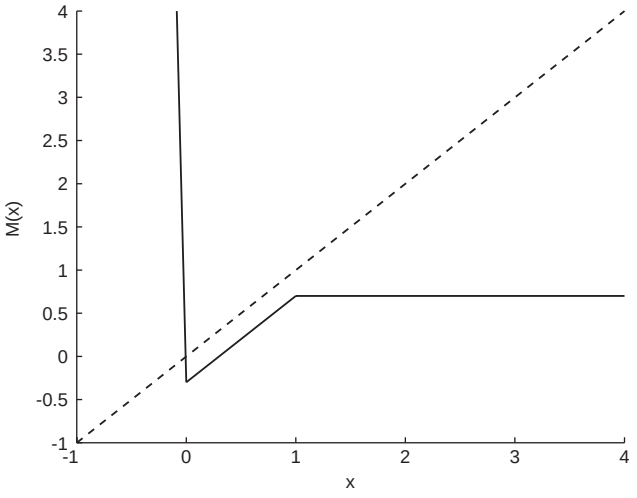

Fig. 14. The piecewise linear map defined by Eq. (6) with $\kappa = -0.3$ and $\alpha = 50$.

Fig. 15 shows regions of existence and stability of Wenckebach rhythms up to order 7:6 although the sequence of higher order Wenckebach rhythms continues in the same manner with an accumulation of rhythms as $\kappa \to 0$ and $\alpha \to \infty$. This infinite sequence would be truncated if the sharp tip were to be made smooth, with the higher order rhythms being replaced by a period doubling cascade. Note that for $\kappa > 0$, the 1:1 rhythm (fixed point) is the only stable rhythm.

In Fig. 15 (top), for each $N \geqslant 2$, there are two $N+1:N$ rhythms to the right of the $N-1$th the solid curve, one stable and one unstable. Each solid curve represents a fold bifurcation along which the pair appears. To the right of the dashed curve, the stable rhythm goes unstable but continues to exist until $\kappa = 0$. The dashed curve represents a flip bifurcation, through which a double Wenckebach rhythm arises: a $2(N+1):2N$ rhythm consisting of an alternating pair of similar but not identical $N+1:N$ rhythms. See the appendix for details on the boundaries of these regions.

It is worth noting that according to the Sarkovskii sequence, at all parameter values between the leftmost solid curve and $\kappa = 0$, there are periodic orbits of all periods (Stefan, 1977). This follows from the fact that 3:2 rhythms, which exist throughout this region, are period three orbits. The outlined regions merely pick out the rhythms with Wenckebach structure.

A summary of the bifurcation diagram for the slow manifold map is given in Fig. 16.

7. Discussion

Despite much success in explaining experimental results from paced cardiac cells and tissue, the APD map approach has certain drawbacks when particular

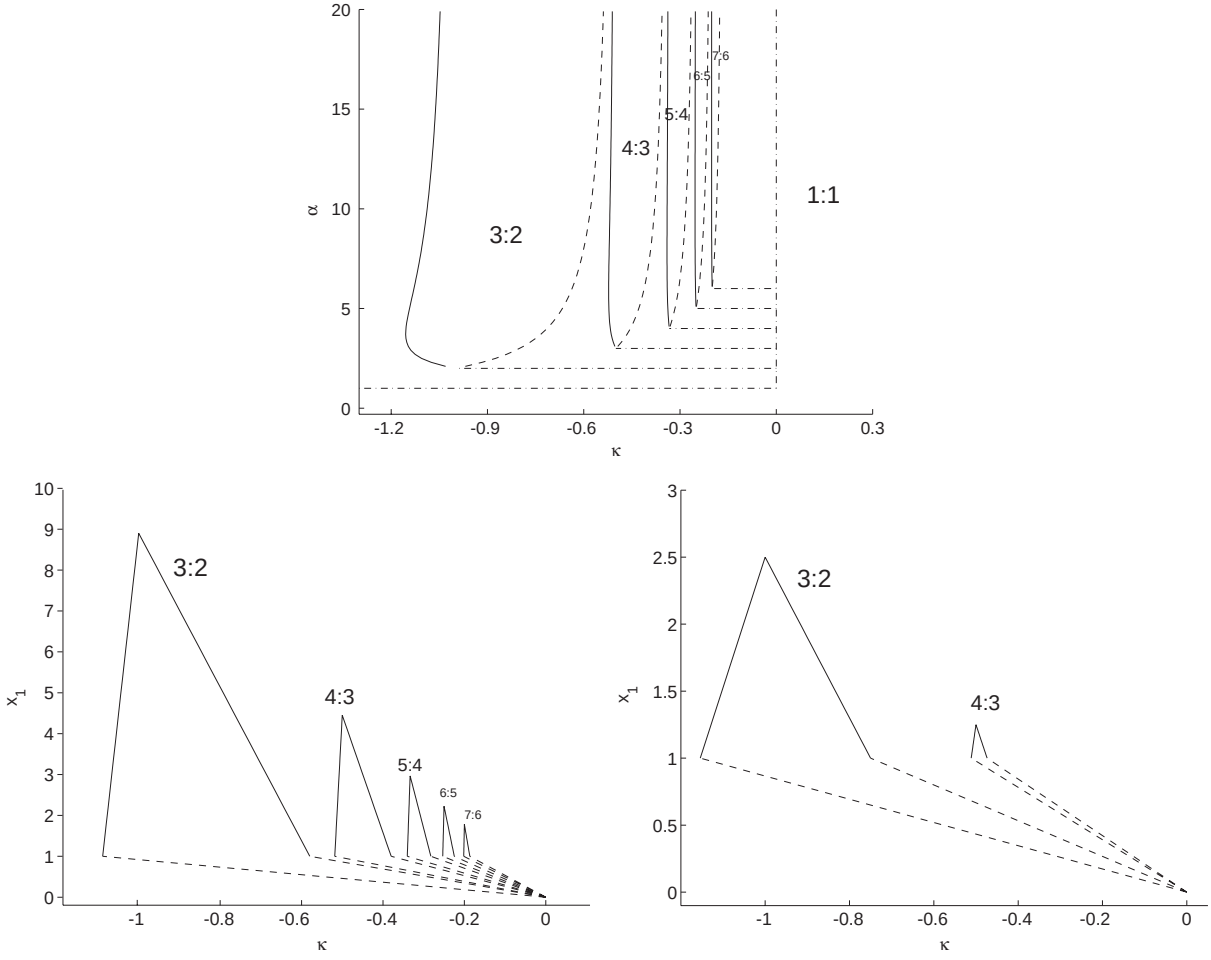

Fig. 15. Bifurcation diagrams for the piecewise linear map M. Top: regions of existence and stability of $N+1:N$ rhythms. Each solid curve represents a fold bifurcation along which a pair of $N+1:N$ rhythms appear. The stable rhythm loses stability along the dashed curve through a flip bifurcation generating a $2(N+1):2N$ rhythm. Two unstable $N+1:N$ rhythms exist above each dash-dotted line. Bottom: two sections of the bifurcation diagram taken at $\alpha = 10$ and 3.5. The value of the largest iterate (x_1, as given in the appendix) is plotted against κ. Solid lines are stable rhythms, dashed lines are unstable. Note that all rhythms disappear at $\kappa = 0$, an artifact of the sharp corner in M. Compare the $\alpha = 10$ case with Fig. 13.

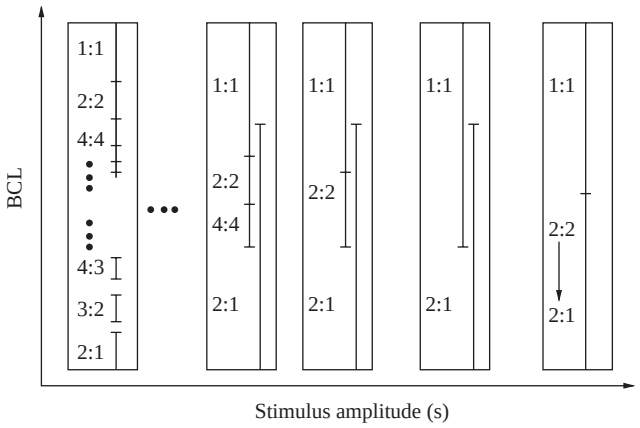

Fig. 16. A summary of the stable rhythms found in the slow manifold map and the parameter ranges (in a qualitative sense) over which they exist. The vertical line segments represent stable rhythms. Overlapping line segments represent bistability, for example, in the fourth box from the left, there is bistability of the 1:1 and 2:1 rhythms. Hash marks represent flip and fold bifurcations. Gaps in the line segment (in the first box) denote regions with more complicated rhythms. Note the gradual appearance of the period doubling cascade exhibiting bistability with the 2:1 rhythm and the lack of bistability in the leftmost box. Wenckebach rhythms are believed to appear only after the period doubling cascade is "complete" and a period three rhythm appears.

issues are addressed. For example, stability predictions based on it are not consistent with experimental observations in a quantitative sense, the map is sometimes not well defined (multivalued), and certain observed rhythms cannot be explained by it. Furthermore, certain parameter dependence is left unexplained (for example, stimulus amplitude) and, as a result, only a partial bifurcation diagram can be constructed leaving some questions unanswered (for example, what determines the transitional rhythms between 1:1 and 2:1 rhythms?). Nonetheless, as a first approximation, it is remarkably useful in understanding the appearance and stability structure of the most predominant rhythms (1:1, 2:2, 2:1) and as a result it has been adopted and generalized in an attempt to patch the holes in the original formulation.

In this paper, an alternate map, which in a sense generalizes the APD map, has been derived directly from an ODE model allowing for more concrete connections to cardiac physiology to be made. The main drawback of the ODE model used in the derivation is that it is not a physiological model and hence does not provide the quantitative accuracy of more detailed ionic models. Surprisingly, the FitzHugh–Nagumo model, in one of its simplest manifestations, can be reduced to a map that closely resembles the traditional APD map, perhaps explaining some of the quantitative failings of the APD map. Once this simplest map is generalized to a second approximation (both figuratively and in the sense of perturbation theory), a more complete understanding of the bifurcation structure can be deduced.

But quantitative prediction based on this improved map are still unlikely to be accurate simply because FHN is not a physiological model and only describes cardiac dynamics in a qualitative sense. Fortunately, the approach taken in deriving the slow manifold map can easily be generalized to a more detailed ionic model based on a few simple assumptions that must be tested. There are two generic structures that are almost certainly present in any cardiac model. The first structure is the slow manifold, along which the state of a cell returns to rest. The second structure is what might best be referred to as the *excitation threshold manifold* which is the manifold that forms the boundary in state space between the region of depolarization ($dv/dt > 0$) and repolarization ($dv/dt < 0$).

In the FHN model, the slow manifold is one-dimensional provided ε is sufficiently small. In an ionic model, the dimension of this manifold depends on the details of repolarization and, in particular, the time constants associated with the Ca^{2+} and K^+ channels. Unfortunately, these time constants are not really constant (due to transmembrane potential dependence) so that careful study is required to determine the dimension of this manifold. Provided this manifold is one-dimensional, there is hope for constructing a one-dimensional slow manifold map. If this manifold is two-dimensional, it ought to be possible to parameterize it by the transmembrane potential variable and one other state variable. This second state variable can be thought of as a memory variable allowing for the formal derivation of a memory map analogous to those proposed by Chialvo and Jalife (1990), Fox et al. (2002) and Otani and Gilmour (1997). In either case, the approach provides a rigorous means of deriving a more quantitative map, whether it be one-, two- or higher-dimensional.

The second structure might loosely be referred to as the excitation threshold. In the FHN model, the middle branch of the v nullcline acts as an excitation threshold, although it is not a true threshold in the sense of all or none excitation, and provides the delay region which is necessary for a non-monotonic, Wenckebach-generating map. For the higher-dimensional ionic models, this middle branch is a hypersurface of the full state space. If one is interested in determining whether Wenckebach rhythms exist for a given model, one must check to see if the slow manifold, when shifted in the v direction by s (the stimulus amplitude), intersects the threshold manifold in such a way as to generate long delays.

The presence and characterization of these two state space structures would provide a rigorous and mechanistic means of exploring the nature of Wenckebach rhythms, elucidating the ionic basis of memory and providing a quantitatively accurate map describing the behavior of paced isolated cardiac cells.

Acknowledgements

This research was supported by Fonds FCAR and by NSF grant No. DMS-99700876 (provided to J.P. Keener, the author's graduate supervisor). The author would like to thank J.P. Keener and B. Peercy for helpful discussions and suggestions.

Appendix A

A.1. Derivation of the log map

Let us examine a theoretical excitable system in which the APD assumption is valid. A similar system was analysed by Othmer et al. in a series of papers that examined existence and stability of 1:1, 2:2 and 2:1 rhythms (Othmer and Watanabe, 1994; Othmer and Xie, 1999; Xie et al., 1996). We use a slightly simpler system for the sake of illustrating some key ideas.

Consider the FHN ODE system with piecewise linear dynamics:

$$\varepsilon\frac{dv}{d\tau} = H(v-a) - v - w, \quad \frac{dw}{d\tau} = v, \tag{A.1}$$

where H is the Heaviside function, ε is a small parameter and a is the excitation threshold. In the singular limit, as $\varepsilon \to 0$, the dynamics are restricted to the upper and lower branches of the v nullcline given by $v = 1 - w$ and $v = -w$, respectively. The slow dynamics along those branches are defined by

$$\frac{dw}{d\tau} = 1 - w, \quad \frac{dw}{d\tau} = -w \tag{A.2}$$

on the upper and lower branch, respectively.

The experimental protocol calls for a periodic stimulus to be applied to the cell which we interpret here as the periodic addition of a delta function scaled by the chosen stimulus amplitude, s, to the v equation. This puts a jump discontinuity in v with an amplitude exactly that of the stimulus (s). In general, the poststimulus state of the system will not be on one of the branches so we must appeal to the fast time scale to determine the evolution. If the poststimulus value of v is less than or equal to a, the state of the cell snaps back to the lower branch. Otherwise, the state jumps to the upper branch. In either case, the value of w is unchanged from the prestimulus value.

As mentioned, we assume that BCL is sufficiently large so that immediately preceding every stimulus the state of the cell is on the lower branch. With this assumption, we construct a map which gives the successive positions of the state of the cell on the lower branch immediately preceding successive stimuli. There are three equivalent ways of keeping track of this position, using successive values of either w, v or APD. The singular limit assumption ensures that the cell spends time only on the upper and lower branches and does not spend time moving between the two. The times spent on these branches are the APD and DI respectively. Solving (A.2) allows us to calculate w_{n+1} as a function of w_n:

$$w_{n+1} = \frac{1-a}{a}e^{-\mathrm{BCL}}(1 - w_n).$$

Equivalently, this map can be expressed in terms of APD:

$$\mathrm{APD}_{n+1} = h(\mathrm{DI}_n) = \ln\left(\frac{1-(1-a)e^{-\mathrm{DI}_n}}{a}\right),$$

where $\mathrm{DI}_n = \mathrm{BCL} - \mathrm{APD}_n$.

If we allow for the possibility that the cell does not recover enough to fire after the first BCL, the cell has $\mathrm{DI}_n = (N+1)\cdot\mathrm{BCL} - \mathrm{APD}_n$ time units before firing where N is the number of failed responses. The interval of APD in which the cell skips N responses can be calculated as a function of the stimulus amplitude, s, and the threshold, a. The minimum DI which allows for a response is the length of time it takes for the cell to recover from $w = 1 - a$ to $w = s - a$. Thus, $\mathrm{DI}_{\min} = \ln((1-a)/(s-a))$ and the interval of APD for which the cell fails to respond N times is given by $J_N = (N\cdot\mathrm{BCL} - \mathrm{DI}_{\min}, (N+1)\cdot\mathrm{BCL} - \mathrm{DI}_{\min})$.

Finally, if the time scale is allowed to differ on the upper and lower branch of the piecewise linear right hand side, the ratio of these time scales, η, can be introduced to the model by replacing the right hand side of the first equation in (A.2) by $(1-w)/\eta$. We have also neglected to give an absolute time scale, call it μ, for the map which is required if it is to be compared to experimental results. With these final modifications, the APD map is given by

$$\mathrm{APD}_{n+1} = h(\mathrm{DI}_n) = \mu\eta\ln\left(\frac{1-(1-a)e^{-\mathrm{DI}_n/\mu}}{a}\right), \tag{A.3}$$

where $\mathrm{DI}_n = (N+1)\cdot\mathrm{BCL} - \mathrm{APD}_n$ and N is determined by satisfying $\mathrm{APD}_n \in J_N$. Due to its logarithmic form, we refer to this map as the log map. Similar functional forms have been derived in a similar manner previously (Karma, 1994; Tolkacheva et al., 2002).

From its development in an experimental context, the choice of APD as the argument for a map is appropriate due to the constraints of measurement. However, a theoretical approach has no such constraints. For the sake of understanding the log map in light of developments in Section 4.1, it is more instructive to represent it in terms of the transmembrane potential v.

With different time scales on the upper and lower branches, the log map can be expressed as

$$v_{n+1} = -e^{-\mathrm{BCL}/\mu}(1-a)\left(\frac{1+v_n}{a}\right)^{\eta},$$

for $v_n > a - s$. For $v_n < a - s$, the stimulus does not elicit a response and so

$$v_{n+1} = v_n e^{-\mathrm{BCL}/\mu}.$$

A.2. Log map parameter dependence

With the map expressed in terms of v_n, we can easily check the influence of the parameters on the stability of the 1:1, 2:2 and 2:1 solutions. To simplify the analysis, we consider the case $\eta = 1$.

If a fixed point exists on the first continuous segment of the map,[3] it must have the form

$$v^* = -\frac{1}{1 + (a/(1-a))e^{BCL}}.$$

Of course, existence of such a fixed point requires that $s > a - v^*$ that is, the stimulus is sufficiently large to elicit a response. Solving for a condition on BCL, existence of a fixed point is guaranteed for

$$e^{BCL} > \left(\frac{1}{s-a} - 1\right)\frac{1-a}{a}.$$

The stability of this fixed point is determined by the slope of the map at the fixed point. Putting the condition for stability into a convenient form, we find that stability of the fixed point is guaranteed for

$$e^{BCL} > \frac{1-a}{a}.$$

Thus, if $s > a + \frac{1}{2}$ then stability is lost before the fixed point disappears and a branch of 2:2 rhythms emerges from the bifurcation point (see Fig. 4).

Conversely, if $s < a + \frac{1}{2}$ then the fixed point disappears before stability is lost and no branch of stable 2:2 rhythms can exist. Thus, the log map agrees with the observation of Yehia et al. (1999) that alternans appear for large stimulus amplitude and are replaced by a direct transition from 1:1 to 2:1 as s decreases, at least in the case of $\eta = 1$. This result extends to the case of $\eta \neq 1$ provided the 2:2 branch emerges from the fixed point through a supercritical bifurcation.

A.3. Connections between the exponential and log maps

One of the failures of the exponential map, (1), is its lack of quantitative agreement with experimental data (Hall et al., 1999; Yehia et al., 1999). The log map, (A.3), is qualitatively similar to the exponential map. In fact, given APD_{max}, A, DI_{min} and τ for g it is not difficult to find η, s, μ and a for h so that h is a good fit to g. Forcing the two maps to have the same DI_{min} and to satisfy

$$\lim_{DI\to\infty} g(DI) = \lim_{DI\to\infty} h(DI), \tag{A.4}$$

allows for the first two parameters to be expressed in terms of μ and a. The problem of fitting the log map to the exponential map is reduced to minimizing the error $\|g - h\|$ over μ and a. An example is given in Fig. 5.

[3] Fixed points on the second segment correspond to 1:0 subthreshold responses. These high-frequency rhythms are beyond the range of interest of this study.

With this fit in mind, the exponential map can be evaluated in terms of the piecewise linear FHN model in the limit $\varepsilon \to 0$. When compared with the modern spectrum of detailed ionic models (Beeler and Reuter, 1977; Courtemanche et al., 1998; Luo and Rudy, 1991, 1994), the FHN model fails to measure up as a quantitative model. The added simplifications of piecewise linear dynamics and the singular limit assumption are almost exclusively considered when purely analytical results are sought, placing the model into the category of "strictly qualitative" by physiological standards. It is not at all surprising that an APD map derived from such a simplified model is limited to the realm of qualitative explanations.

Appendix B

Recall the definition of the piecewise linear map given in (6):

$$M(x) = \begin{cases} M_1(x) = -\alpha x + \kappa, & x \leqslant 0, \\ M_2(x) = x + \kappa, & 0 < x \leqslant 1, \\ M_3(x) = 1 + \kappa, & x > 1. \end{cases} \tag{B.1}$$

In order to calculate Wenckebach rhythms, there are four cases that must be considered. Each case can be identified with a region of parameter space by writing down the appropriate conditions on the successive iterates of $\mathscr{M}$. The following list includes a description of each region along with inequalities that bound the region and the value of the first iterate. The four cases are:

1. A stable $N+1:N$ Wenckebach rhythm with 1 beat on the M_3 interval, $N-1$ beats on the M_2 interval and one beat on the M_1 interval:

$$-k > \frac{1+\alpha}{\alpha N - 1}, \quad -k < \frac{1}{N-1},$$

$$x_1 = -\alpha - \alpha N k + k.$$

2. A stable $N+1:N$ Wenckebach rhythm with 1 beat on the M_3 interval, $N-2$ beats on the M_2 interval and two beats on the M_1 interval:

$$-k < \frac{\alpha^2 - 1}{\alpha^2(N-1) - \alpha + 1}, \quad -k > \frac{1}{N-1},$$

$$x_1 = \alpha^2 + (\alpha^2(N-1) - \alpha + 1)k.$$

3. An unstable $N+1:N$ Wenckebach rhythm with N beats on the M_2 interval and one beat on the M_1 interval:

$$-k < \frac{1+\alpha}{\alpha N - 1}, \quad \alpha > N,$$

$$x_1 = -\frac{\alpha N - 1}{1+\alpha}k.$$

4. An unstable $N+1:N$ Wenckebach rhythm with $N-1$ beats on the M_2 interval and two beats on the M_1 interval:

$$-k < \frac{\alpha^2 - 1}{\alpha^2(N-1) - \alpha + 1}, \quad \alpha > N,$$

$$x_1 = -\frac{\alpha^2(N-1) - \alpha + 1}{\alpha^2 - 1} k.$$

References

Beeler, G.W., Reuter, H.J., 1977. Reconstruction of the action potential of ventricular myocardial fibers. J. Physiol. 268, 177–210.

Cherry, E.M., Fenton, F.H. Suppression of alternans and conduction blocks despite steep apd restitution: electrotonic, memory and conduction velocity restitution effects. Am. J. Physiol Heart Circ. Physiol, 2004.

Chialvo, D.R., Jalife, J., 1990. Cardiac Electrophysiology: from Cell to Bedside, On the non-linear equilibrium of the heart: locking behavior and chaos in Purkinje fibers. 1st Edition. Saunders, London, pp. 201–214.

Coombs, S., Osbaldestin, A.H., 2000. Period adding bifurcations and chaos in a periodically stimulated excitable neural relaxation oscillator. Phys. Rev. E 62, 4057–4066.

Courtemanche, M., Glass, L., Keener, J.P., 1993. Instabilities of a propagating pulse in a ring of excitable media. Phys. Rev. Lett. 70, 2182–2185.

Courtemanche, M., Ramirez, R.J., Nattel, S., 1998. Ionic mechanisms underlying human atrial action potential properties: insights from a mathematical model. Am. J. Physiol. 275, H301–H321.

Cytrynbaum, E.M., Keener, J.P., 2002. Stability conditions for the traveling pulse: modifying the restitution hypothesis. Chaos 12 (3), 788–799.

Delmar, M., Glass, L., Michaels, D.C., Jalife, J., 1989a. Ionic basis and analytical solution of the wenckebach phenomenon in guinea pig ventricular myocyte. Circ. Res. 65, 775–788.

Delmar, M., Michaels, D.C., Jalife, J., 1989b. Slow recovery of excitability and the wenckebach phenomenon in the single guinea pig ventricular myocyte. Circ. Res. 65, 761–774.

Echebarria, B., Karma, A., 2002. Instability and spatiotemporal dynamics of alternans in paced cardiac tissue. Phys. Rev. Lett. 88(20) 208101-1–208101-4.

Elharrar, V., Surawicz, B., 1983. Cycle length effect on restitution of action potential duration in dog cardiac fibers. Am. J. Physiol. 244, H782–H792.

Fenton, F., Cherry, E.M., Hastings, H.M., Evans, S.J., 2002. Multiple mechanisms of spiral wave breakup in a model of cardiac electrical activity. Chaos 12 (3), 852–892.

Fox, J.J., Bodenschatz, E., Gilmour Jr., R.F., 2002. Period-doubling instability and memory in cardiac tissue. Phys. Rev. Lett. 89(13) 138101-1–138101-4.

Gilmour Jr., R.F., 2002. Electrical restitution and ventricular fibrillation: negotiating a slippery slope. J. Cardiovasc. Electrophysiol. 13, 1150–1151.

Guevara, M.R., Ward, G., Shrier, A., Glass, L., 1984. Electrical alternans and period-doubling bifurcations. In: Computers in Cardiology. IEEE Computer Society, Silver Spring, MD, pp. 167–170.

Guevara, M.R., Jeandupeux, D., Alonso, F., Morissette, N., 1989. Wenckebach rhythms in isolated ventricular heart cells. In: Pnevmatikos, St., Bountis, T., Pnevmatikos, Sp. (Eds.), International Conference on Singular Behavior and Nonlinear Dynamics, 1st Edition. Vol. 2. World Scientific Publishing Co. Pte. Inc., Singapore, pp. 629–642.

Hall, G.M., Bahar, S., Gauthier, D.J., 1999. Prevalence of rate-dependent behaviors in cardiac muscle. Phys. Rev. Lett. 82 (14), 2995–2998.

Ideker, R.E., Rogers, J.M., Gray, R.A., 2002. Steepness of the restitution curve: a slippery slope? J. Cardiovasc. Electrophysiol. 13, 1173–1175.

Karma, A., 1994. Electrical alternans and spiral wave breakup in cardiac tissue. Chaos 4, 461–472.

Karma, A., 2000. New paradigm for drug therapies of cardiac fibrillation. Proc. Natl. Acad. Sci. 97 (11), 5687–5689.

Lewis, T.J., Guevara, M.R., 1990. Chaotic dynamics in an ionic model of the propagated cardiac action potential. J. Theor. Biol. 146, 407–432.

Li, T., Yorke, J.A., 1975. Period three implies chaos. Am. Math. Monthly 82 (10), 985–992.

Luo, C.H., Rudy, Y., 1991. A model of the ventricular cardiac action potential; depolarization, repolarization and their interaction. Circ. Res. 68, 1501–1526.

Luo, C.H., Rudy, Y., 1994. A dynamic model of the cardiac ventricular action potential; I: simulations of ionic currents and concentration changes. Circ. Res. 74, 1071–1096.

Nolasco, J.B., Dahlen, R.W., 1968. A graphic method for the study of alternation in cardiac action potentials. J. Appl. Physiol. 25 (2), 191–196.

Otani, N.F., Gilmour Jr., R.F., 1997. Memory models for the electrical properties of local cardiac systems. J. Theor. Biol. 187 (3), 409–436.

Othmer, H.G., Watanabe, M., 1994. Resonances in excitable systems under step-function forcing. i. harmonic solutions. Adv. Math. and Appl. 4, 399–441.

Othmer, H.G., Xie, M., 1999. Subharmonic resonance and chaos in forced excitable systems. J. Math. Biol. 39, 139–171.

Panfilov, A.V., Zemlin, C.W., 2002. Wave propagation in an excitable medium with a negatively sloped restitution curve. Chaos 12 (4), 800–806.

Qu, Z., Weiss, J.N., Garfinkel, A., 1997. Spatiotemporal chaos in a simulated ring of cardiac cells. Phys. Rev. Lett. 78 (7), 1387–1390.

Stefan, P., 1977. A theorem of sarkovskii on the existence of periodic orbits of continuous endomorphisms of the real line. Commun. Math. Phys. 54, 237–248.

Tolkacheva, E.G., Schaeffer, D.G., Gauthier, D.J., Mitchell, C.C., 2002. Analysis of the fenton karma model through an approximation by a one-dimensional map. Chaos 12 (4), 1034–1042.

Tolkacheva, E.G., Schaeffer, D.G., Gauthier, D.J., Krassowska, W., 2003. Condition for alternans and stability of the 1:1 response pattern in a memory model of paced cardiac dynamics. Phys. Rev. E 67, 031904-1–031904-10.

Watanabe, M., Otani, N.F., Gilmour Jr., R.F., 1995. Biphasic restitution of action potential duration and complex dynamics in ventricular myocardium. Circ. Res. 76, 915–921.

Xie, M., Othmer, H.G., Watanabe, M., 1996. Resonance in excitable systems under step-function forcing. ii. subharmonic solutions and persistence. Physica D 98, 75–110.

Yehia, A.R., Shrier, A., Lo, K.C.-L., Guevara, M.R., 1997. Transient outward current contributes to wenkebach-like rhythms in isolated rabbit ventricular cells. Am. J. Physiol. 273, H1–H11.

Yehia, A.R., Jeandupeux, D., Alonso, F., Guevara, M.R., 1999. Hysteresis and bistability in the direct transition from 1:1 to 2:1 rhythm in periodically driven single ventricular cells. Chaos 9 (4), 916–931.